Applied Journal of Physical Science
Volume 6(1), pages 1-12, February 2025
Article Number: C8B5919F1
ISSN: 2756-6684
https://doi.org/10.31248/AJPS2024.109
https://integrityresjournals.org/journal/AJPS

Full Length Research

Structural, physical and passive radiation shielding efficiency of bismuth ore and barium oxide doped sand-sourced glasses

Jibrin Suleiman Yaro[1,2]*, Aliyu Abubakar Sadiq[1], Aliyu Umar Sa'ad[1], Hamza Abdulkarim Muhammad[1], Jamilu Ari Labaran[1,3], Ali Musa Kazzayo[1,3], Ibrahim Abullahi Ode[1,2] and Lawal Abdullahi[1,4]

[1]Department of Physics, Federal University of Lafia Nasarawa State, Nigeria.
[2]Department of Physics, Federal University of Technology Owerri Imo State, Nigeria.
[3]Isa Mustapha Agwai Polytechnic Lafia, Nasarawa State, Nigeria.
[4]Department of Chemistry, Federal University of Technology Owerri Imo State, Nigeria.

*corresponding author. Email: jibrinyarsuleiman@gmail.com

Received 13th November 2024; Accepted 15th January 2025

ABSTRACT: Concrete and lead-based aggregates are communal shielding materials against penetrating radiations, X-rays and gamma photons. Conversely, lead is expensive and chemically hazardous, and concrete ages become opaque. The continuous search for alternative radiation shielding materials has been motivated. Nigerian small-scale mining has produced mineral ores that contain glass sand and bismuth ore. Analysis revealed that 85.20% of the bismuth ore and glass sand was composed of 78.99% silica. Glass sand-sourced silica was used to create the innovative glass series, which also contained bismutite and barium oxide as dopants to change the glass's desired characteristics. The glass series was fabricated using the melt quenching method, having the empirical chemical formula (100-y) {85[25(glasssand) + 35B_2O_3+40Na_2CO_3] + 15BaO}y[$Bi_2O_2CO_3$], where $5 \leq y \geq 25\ wt.\%$. The novel glass was characterized using measurements. The density of the glass increased from 2.919 to 3.532 g/cm^3. The refractive index value range of the glass system is 2.23-2.49. The glasses were confirmed amorphous as the XRD pattern revealed, whereas the FTIR analysis showed the presence of BO_3 and SiO_4 structural units. The Gamma-Ray experiment was carried out on all glass samples using two radioactive gamma point sources, namely, Caesium-137 and Co-60, the results show that the LAC decreases and increases at different weight percentages ranging from 5 to 25%, GLS25 have the highest LAC while the least LAC was observed at GLS15 for the two gamma source. MAC of the glass system, as the content of $Bi_2O_2CO_3$ changes from 5 to 25 wt. %, the values of MAC at energy (661KeV) and energy (1235KeV) show a similar decreasing and increasing behaviour as exhibited by LAC. The observed increase in MAC of the prepared glasses might be linked with an increase in glass effective density as well as mass density, which thereby results in a high probability of photon interaction. The values of HVL and TVL for Caesium-137 increase from 2.449954 to 5.344431 cm then decrease to 2.046755 cm (HVL) and 8.138571 cm to 17.75381cm to 6.799175 cm (TVL), respectively. These results show that the samples doped with a greater wt. % of $Bi_2O_2CO_3$ have the lowest HVL and TVL values for Caesium-137 and Cobalt-60. A drop in HVL and TVL for the two gamma sources is a direct result of a density increase. HVL and TVL values are lower in good shielding materials. The MFP for both Cobalt-60 and Caesium-137 is comparable to HVL and TVL. With the exception of GLS15, which has the highest MFP (8.64259 cm) for Caesium-137 and the lowest MFP (2.952844 cm) for Cobalt-60, the MFP values decrease as the amount of $Bi_2O_2CO_3$ increases. It also has the greatest LAC and density values among the created glass samples. It is shown that the innovative glasses have higher performance in radiation shields.

Keywords: Glass sand, Bismutite, Barium Oxide, XRD, FTIR, Radiation shielding parameters, Gamma rays radiation.

INTRODUCTION

Ionizing radiation is been used progressively in diagnostic and therapeutic medicine. However, people can encounter the effect of exposure to ionizing radiation which is dangerous to both exposed patients and clinicians. Therefore, there is a need to enforce radiation protection regulations in facilities where sources of radiation are handled. Countries across the globe have promogulated laws and regulations guiding the handling and using radiation sources in hospitals and other industries (Baptista Neto and Faria, 2014; Sekimoto and Katoh, 2015).

Some of the effects of radiation exposure are radiation illness, tumour, transmutation, and even death. It is obvious that this is the most important problem compelling the needed protections to limit exposure to radiation through the use of passive shields in order to protect personnel and patients at a hospital (Al-Buriahi *et al.,* 2020; Alazoumi *et al*., 2017; Obaid *et al.,* 2018).

Radiation shielding is the science and practice of limiting harm to human beings and the environment from the effects of ionizing radiation. Radiation exposure is the foremost uncertainty when setting up nuclear power plants, which require the use of resilient radio-isotopes which include food conservation and tumour handling, particle accelerator services, so also in diagnostic techniques to prevent radiation from causing harm to personnel and patients (Gaikwad *et al*., 2018; Kolanoski and Wermes, 2020; Kumar *et al.,* 2020). Different types of protective devices have been installed in radiology facilities in order to protect patients and personnel (Acevedo-Del-castillo *et al*., 2021; IAEA, 2019; Lacomme *et al.,* 2021).

Lead is one of the important shielding materials that's used in the production of radiation shielding glass due to its high atomic number (Z), high density, high stability, and easy process. However, lead toxicity harms the environment and it is one of the leading carcinogens. Therefore, attempts are being made to replace lead with other high atomic number metals in the fabrication of shielding glasses (Bale *et al*., 2008; Baptista Neto and Faria, 2014; Berwal *et al*., 2017a; McCaffrey *et al*., 2007; Sarachai *et al.*, 2018; Singh *et al.,* 2008). Nevertheless, a broad literature search revealed that Glass sand along with bismuth clayey (ore) and barium oxide-based glasses are yet to be fully investigated as potential replacements for lead-based glasses in radiation shielding. These alternative materials have lower effective density; however, they are often efficient shields (Deepty *et al.,* 2019).

The objectives of this paper are to synthesize (100-y){85[25(glass sand)+35H_3BO_3+40Na_2CO_3] +15BaO}y[$Bi_2(CO_3)O_2$], of glass system, analyze the glass system's structural and physical properties and to estimate the radiation shielding properties (HVL, LAC, MAC) of the glass system experimentally using gamma source point. This work aims to fabricate and study the structural and radiation shielding efficiency of the new glass series.

THEORY BASIS

The Linear Attenuation Coefficient μ (cm-[1])

Linear attenuation coefficient (μ) describes the fraction of photons removed from a mono-energetic beam of x-rays or gamma rays per unit thickness of the material (NDT, 2017). The beam passes through the material, the intensity of the beam will be attenuated according to Beer–Lambert's law

$$I=l_o e^{-\mu x} \quad (1)$$

I= the intensity of photons transmitted across some distance X
I_O= the initial intensity of photons.
μ=the linear attenuation coefficient
X= the thickness of the material

Half Value Layer (HVL)

The half-value layer is defined as the thickness of the absorbing material that reduces the beam's intensity to half of its original magnitude. The lower the value of HVL, the better the radiation shielding property in terms of thickness necessity (NDT, 2017). Half value layer is calculated by the relation given below.

$$HVL = ln\frac{2}{\mu} = \frac{0693}{\mu} \quad (2)$$

Where μ is the linear attenuation coefficient

Mean Free Path (MFP)

The mean free path is the average distance a photon can travel in the material before interacting (NDT, 2017). The mean free path has been determined from the linear attenuation coefficient (μ) by the relation.

$$\text{MFP} = \frac{1}{\mu} \quad (3)$$

Glass fabrication

Series of glasses with the chemical formula ((100-y){85[25(glass sand)+35H_3BO_3 +40Na_2CO_3]+15BaO}y[$Bi_2(CO_3)O_2$]), where y is the weight percentage (y= 5, 10, 15, 20, 25%) of bismuth clayey dopant in the glass matrix was fabricated by using a melt-quenching method. Powdered glass sand was the source of silica in this chemical composition.

The powdered samples were weighed based on the proportion in the empirical chemical formulas using electronic balance by Adam PW 184 with serial number

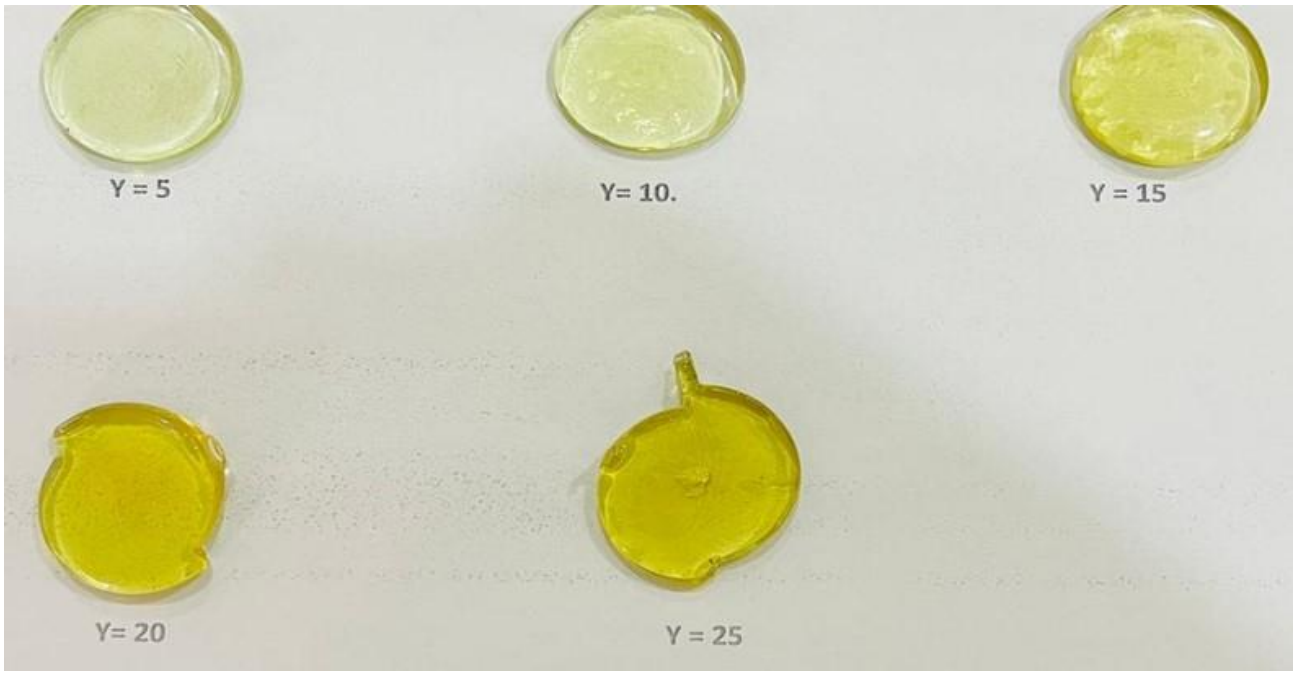

Figure 1. Composition for y = 5,10,15,20 and 25 with empirical formula (100-y){85[25(glass sand)+35H_3BO_3+ 40Na_2CO_3]+15BaO}y[$Bi_2(CO_3)O_2$] of the glass system.

(180x0.0001g) AE437713. The weighed chemicals were then mixed and stirred for about 30 minutes in a clean alumina crucible to get a homogeneous mixture (Causin *et al.,* 2010; Deepty *et al.,* 2019; Aliyu *et al*., 2018). The mixture was then preheated at 400°C for 1 hour to remove moisture, particularly because of the hygroscopic B_2O_3 (Abdul Aziz *et al.,* 2015; Gaikwad *et al.,* 2018). The preheated mixture was immediately transferred to another furnace for melting at 930°C for two hours. After melting, the molten glass casted into a preheated mold before it was then annealed at 450°C for at least one hour in order to remove thermal stress and bubbles (Naseer *et al*., 2021; Aliyu *et al*., 2018). Finally, the thickness of the glass was measured using a digital digimatic vernier caliper with model number HPM After cutting and measuring the glasses, the glasses were then polished using a smooth surface silicon carbide paper (6 cm x 2 cm) to give the glasses a mirror finishing. Fabricated glasses are shown in Figure 1 (Aliyu *et al*., 2018).

Gamma-ray radiation shielding measurements

The experimental measurement of gamma-ray radiation attenuation of the new glass systems was investigated to ascertain shielding effectiveness using two radioactive gamma point sources, namely, Caesium-137 and Co-60, based on the geometry of the laboratory transmission experimental set-up, as depicted in Figure 2a and b and Figure 3a and b. The technical specifications of both sources and detectors used for the experiment are presented in Table 1 and Table 2, respectively.

The distance of separation between the point source and detector was maintained at 32 cm.

It is pertinent to state that the background radiation in the laboratory was measured with a RADOS survey meter (0.10 µSv/hr) before the commencement of measurements. This value was subtracted from all the measurements to ensure the reliability and accuracy of the results. The readings for count rate and dose rates were taken before and after placing the samples in the set-up. Each sample measurement was repeated 3 times, and the average values were recorded. The initial dose rate (also initial intensity) (Io) was measured without any sample placed in between the source and the detector. Afterwards, the reading of the final intensity (I) was recorded, after placing the sample in between the two collimators.

Density measurement of the synthesized glasses

The density of the glass samples prepared in this study was measured using the electronic densimeter MH-300A, with a model number (2023.04.10), and serial number (50.20230409001-2). It has a precision of 0.001 g with a capacity of measuring up to 300 g by Alfa Mirage Company. The instrument works on the Archimedes principle by liquid suspension. Distilled water was used as the immersion liquid, measurement was carried out under normal ambient conditions (Doweidar *et al.,* 2005).

The densities of the prepared glasses were obtained

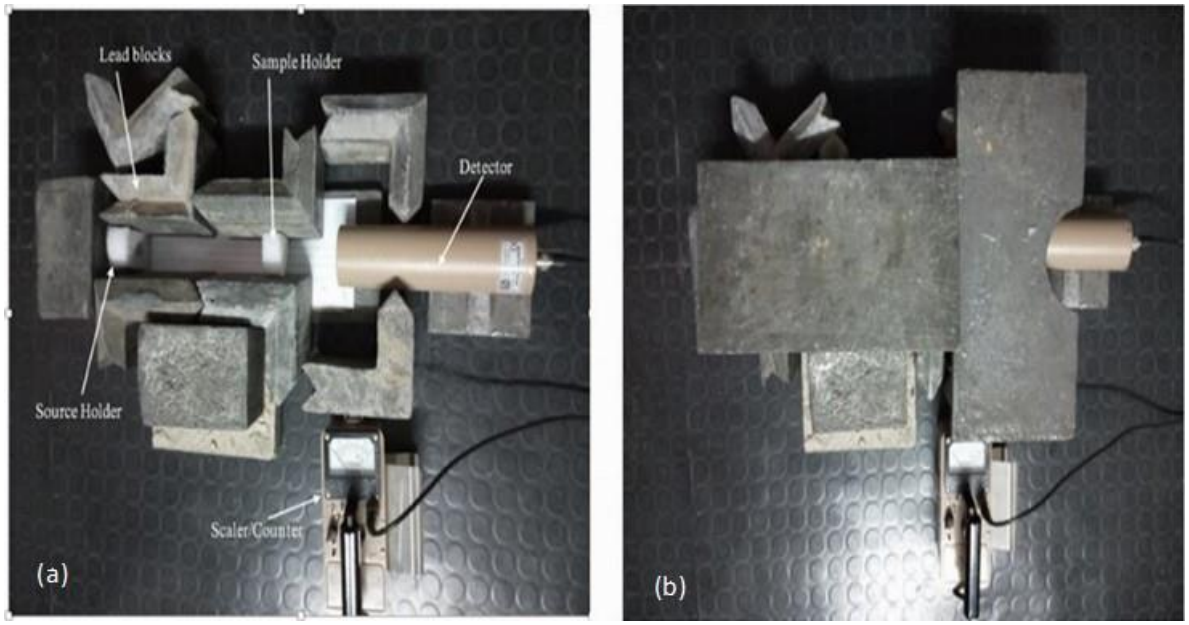

Figure 2. Experimental set-up for gamma ray attenuation using Ludlum NaI Scaler Counter.

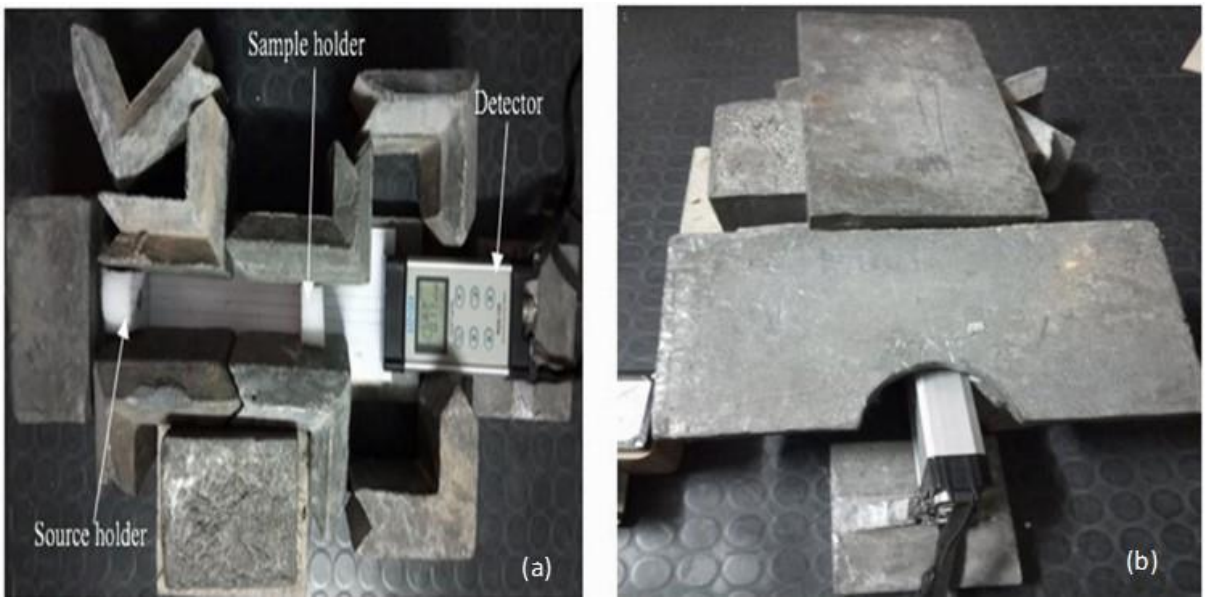

Figure 3. Set-up for gamma ray attenuation using RADOS Survey Meter (RDS-120).

using Eq. 4 by measuring the sample weight in distilled water and air. Measurements were performed 5 times, and the average reading was recorded.

$$\rho = \rho_{\text{Liquid}} \frac{w_{\text{air}}}{w_{\text{air}} - W_{\text{liquid}}} \quad (4)$$

Where w_{air} is the sample weight in air, liquid, and ρ_{liquid} is the density of the liquid used in the experiment. Distilled water was used in density measurements.

XRD analysis of the synthesized glasses

X-ray diffraction (XRD) is a powerful non-destructive technique used to characterize and determine crystalline materials' internal structure. It offers information on structures, phases, texture, and other structural parameters, such as average grain size, crystallinity, inorganic compounds, strain, and crystal defects (Andreeva *et al*., 2011; Bunaciu *et al*., 2015; Connolly, 2005; Dutrow, 2020).

Table 1. Gamma-ray sources and specifications.

Radionuclide	Energy (keV)	Half-life (years)	Initial Activity (A0)	Date of Manufacture
Caesium-137	661.7	30.14	1110 MBq	6th November 2000
Cobalt-60	- 1173.2; - 1332.5 (mean effective energy= 1253 keV)	5.27	1480 MBq	6th November 2000

Table 2. Instruments and measurement specifications.

Gamma source	Caesium-137 (Cs-137) Cobalt-60 (Co-60)
Types of detector	• RADOS Survey Meter (RDS-120), which gives a dose rate (0.05 μSv/hr – 10 Sv/hr) • NaI (Tl) scintillation detector (Ludlum Survey Meter Model 44-10), which gives count rate in units of Counts/min (C/m)
Source-to-detector distance	32 cm
Measurement time	60 seconds

Fourier Transform Infrared Spectroscopy (FTIR)

Fourier transform infrared spectroscopy (FTIR) is a device that mostly offers quantitative and qualitative analysis for organic, inorganic samples, unknown identification, and impurities screening (Causin *et a*l., 2010; Rachniyom *et al.,* 2014). It aids in detecting chemical bonds in a molecule by producing an infrared absorption spectrum of a solid, liquid or gas. The spectra produce a shape of the sample, a distinctive molecular pattern employed to screen and scan samples for numerous diverse components (Chanthima *et al*., 2011; Kumar *et al*., 2020). It is used as an effective investigative device for detecting functional groups and characterizing covalent bonding information in glass science and technology.

RESULTS AND DISCUSSION

Characterizations of Bismutite and glass sand ores

Energy Dispersive X-ray Fluorescence (EDXRF) revealed the two ores contain ~60 wt% Bi and ~78.96 wt% Si, which denotes Bi-O and The Bi ore contained C, O, V, Cu, Al and Si, while the Glass Sand sample metallic oxides are presented in Table 3.

In Table 3 the EDXRF revealed that the glass sand contains 89.738% silica which is needed as glass former and some traces of metallic oxide impurities.

Physical and structural properties of the glasses

The influence of $Bi_2(CO_3)O_2$ addition on the physical characteristics of the fabricated glasses was investigated. The results of the density (ρ) of the glasses computed using Eq. 4 are presented in Table 4. As observed, there is a slight increase in density from 2.92 to 3.53 g/cm^3, which is confirmed by the slight rise in glass density with increasing value of y in the composition formula, as shown in Figure 4.

Figure 4 shows the density of the glasses. The results showed that the density increased with increasing $Bi_2(CO_3)O_2$ from 5 to 25 wt. %. The increase in density from 2.92 to 3.53 g/cm^3 could be attributed to the heavy molar mass of bismuth (208.98 g/mol and 1.03 Å) (Kumar *et al*., 2020). Though barium oxide was also used as a modifier to enhance the networking but kept constant. The observed trend could also be ascribed to the formation of new linkages in the glass matrix on the addition of $Bi_2(CO_3)O_2$, which may have contributed to the volume expansion.

X-ray diffraction (XRD)

Figure 5 shows the XRD spectra of the glass sand-doped bismuth ore and barium oxide glass system. There are no obvious sharp peaks in the pattern. The substance under investigation is amorphous and glassy, as shown by the existence of only a broad hump at an angle of 20 to 35 degrees. The lack of strong peaks indicates that the material does not contain any crystalline phase (Alazoumi *et al.*, 2017; Berwal *et al*., 2017a; Jawad *et al*., 2019; Aliyu *et al.,* 2018).

Fourier transform infrared spectroscopy (FTIR)

Figure 6 shows the FTIR spectra absorption bands at 1383 cm^{-1} and 750-948 cm^{-1} for the synthesised glasses. Thus, the spectra of 750–948 cm^{-1} show a broad, sharp band with a medium-intensity signal, falling inside the O–H band, but the spectra of 1383 cm^{-1} show a sharp band with a low-intensity signal. Peaks corresponding to B-O stretching vibrations in BO_3 units in boroxol rings are responsible for the absorption peaks in the 750–948 cm^{-1} range (Al-Buriahi *et al*., 2020; Sayyed *et al*., 2019).

Table 3. Chemical constituent in the glass sand collected Shabu, Lafia LGA.

Element (Oxide)	Amount /percentage (%)	
	Raw result	Normalized result
Fe_2O_3	0.6139	0.698
SiO_2	78.963	89.738
AL_2O_3	4.825	5.483
MgO	1.45	1.648
P_2O_5	0.2755	0.313
K_2O	0.6736	0.766
SrO	0.368	0.418
Nb_2O_5	0.1249	0.142
Bi_2O_3	0.2252	0.256
BaO	0.4738	0.538

Table 4. Density (ρ) of the glass system.

Bismutite=Y (wt. %)	Density=ρ (gcm^{-3})
5	2.919
10	3.032
15	3.182
20	3.388
25	3.532

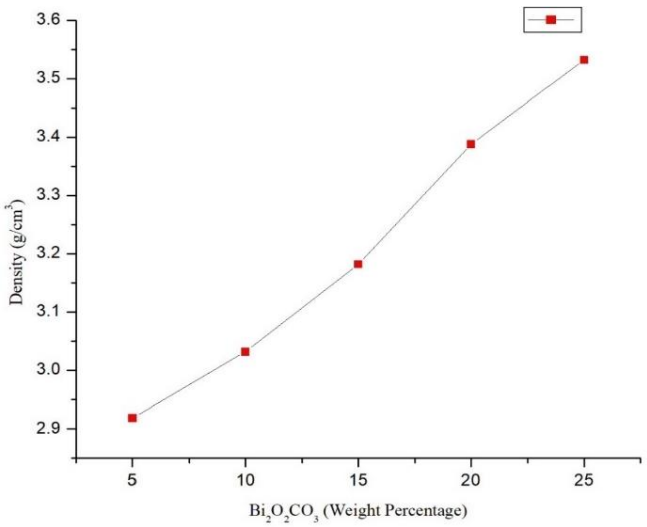

Figure 4. Density against weight percentage of Bismuth ore (Bismutite).

However, stretching vibrations in B-O bonds may be linked to the 1383 cm^{-1} characteristic band that could be associated with B-O bond stretching vibrations (Halimah *et al.,* 2019; Sarachai *et al*., 2018). Bond vibration is represented by the absorption 750-948 cm^{-1}(Aliyu *et al.,* 2018). The bending vibrations are responsible for the IR absorption in the 750–948 cm^{-1} region. As the concentration of Bi_2O_3 in the glass system increased, so did the intensity of absorption.

Gamma-ray attenuation parameters

As earlier stated, two-point sources were used in the experiments to determine the variation of μ (cm^{-1}) measured based on Eq. (5), which is a measure of how much the intensity of the radiation decreases as it passes through a material (Han *et al*., 2021; Naseer *et al.,* 20210) and the mass attenuation coefficient is determined as shown in Eq. 6 (Berwal *et al.,* 2017a). In the study involving Cs-137 (661.7 KeV), the mass attenuation coefficient (MAC) for the fabricated glasses increased with the addition of the dopants. Similar findings have been reported in the literature for Bi_2O_3 doped glasses (Al-Buriahi *et al*., 2020).

$$ln\left(\frac{I}{I_o}\right) = \mu x \quad (5)$$

Where μ is LAC measured in cm^{-1} and MAC of the atom is

$$\text{MAC} = \frac{\mu}{\rho} \quad \text{measured in } cm^2/g \quad (6)$$

Figure 7, Tables 5 and 6 illustrate the variation of LAC as a function of the bismuth ore (bismutite) $Bi_2O_2CO_3$ weight percentage of the glass system at 661 KeV and 1253 KeV. LAC values for GLS5, GLS10, GLS15, GLS20 and GLS25 are 0.198255, 0.198255, 0.115706, 0.246322 and 0.268437 cm^{-1} for caesium-137 and GLS5, GLS10, GLS15, GLS20 and GLS25 are 0.282923, 0.277113, 0.129695, 0.239971 and 0.338657 cm^{-1} for cobalt-60, respectively. It shows non-linear behaviour as a result of a continued rise in bismutite content (Bunaciu *et al.,* 2015; Mariyappan *et al*., 2018). The LAC values increased from 0.115706 to 0.268437 cm^{-1} for caesium-137 and 0.129695 to 0.338657 cm^{-1} for cobalt-60*,* by varying the weight percentage of bismuth ore (bismutite) from 5 to 25%. The LAC decreases and increases at different weight percentages ranging from 5 to 25%, GLS25 for the two sources have the highest LAC (0.268437 and 0.338657 cm^{-1}) while the least LAC was observed at GLS15 for the

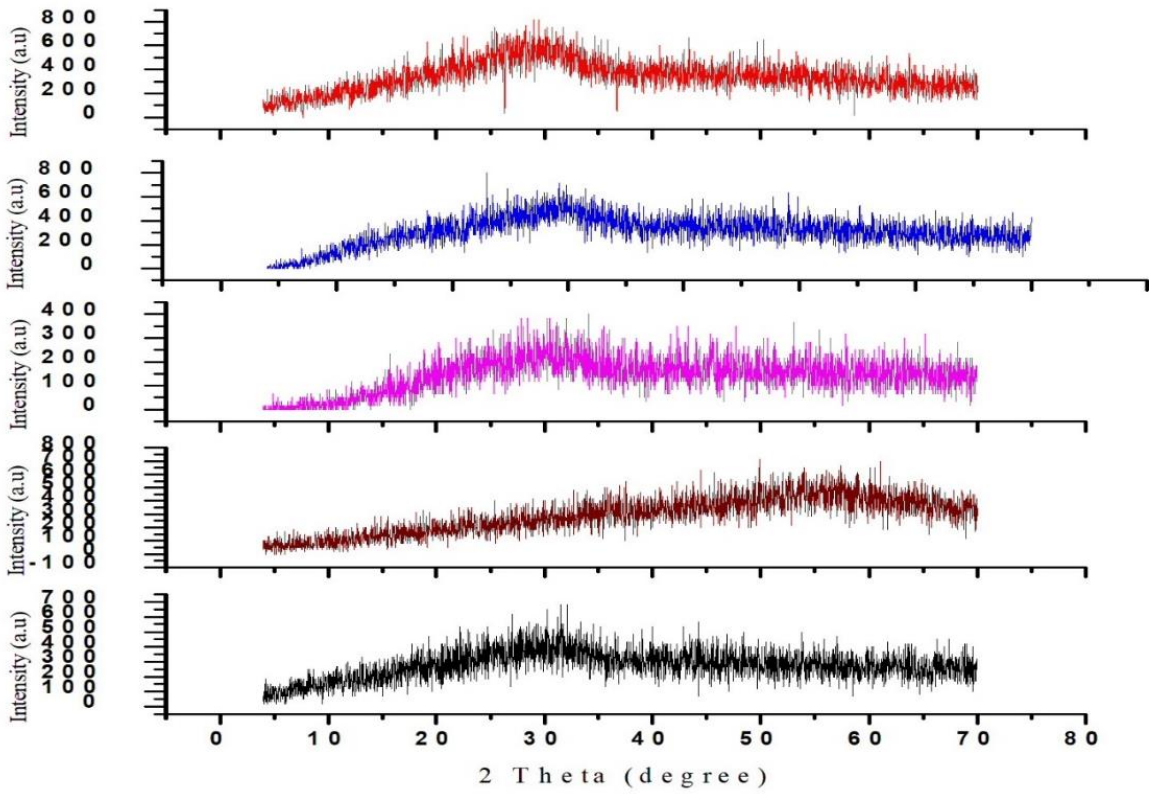

Figure 5. XRD pattern for (100-y){85[25(glass sand)+35H_3BO_3+40Na_2CO_3]+15BaO}y[$Bi_2(CO_3)O_2$] of the glass system.

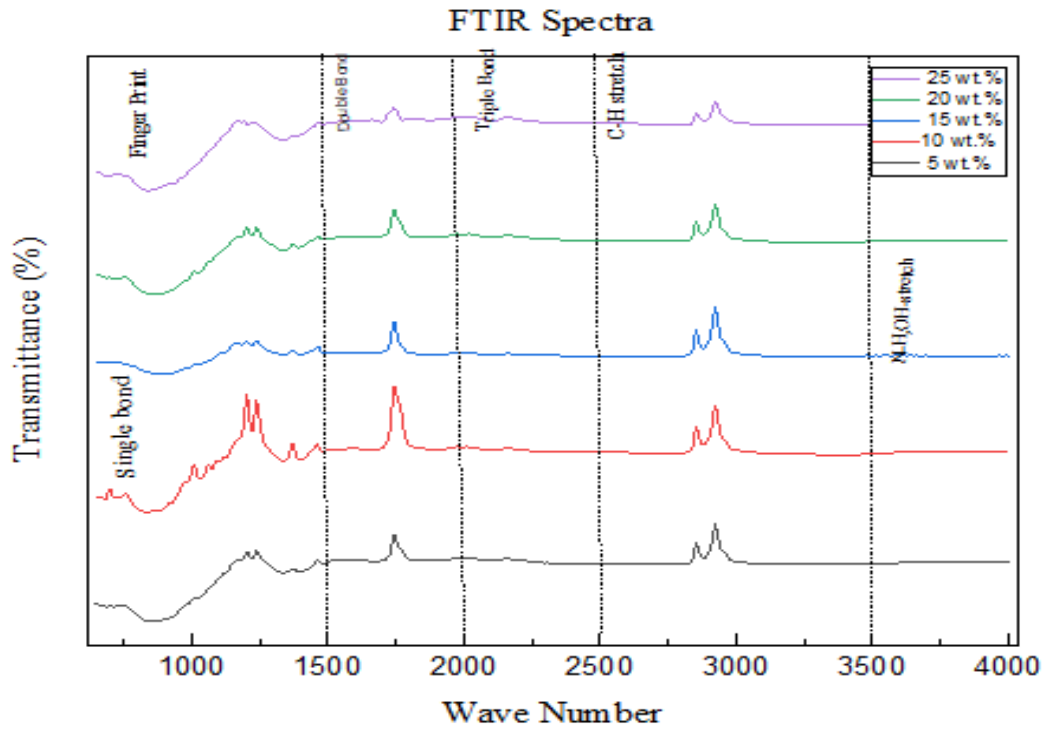

Figure 6. FTIR Pattern for (100-y){85[25(glass sand)+35H_3BO_3+40Na_2CO_3]+15BaO}y[Bi_2 $(CO_3)O_2$] of the glass system.

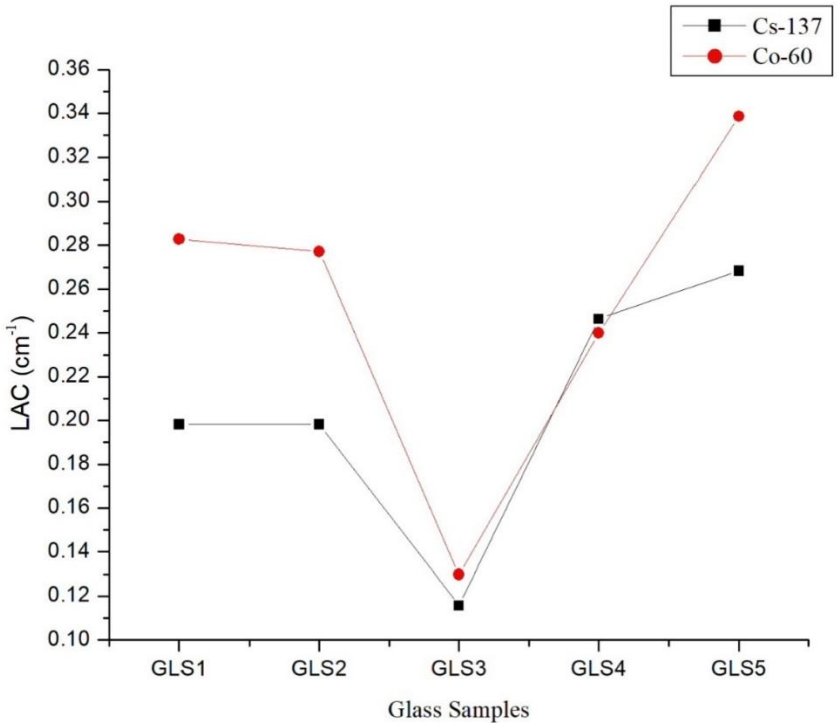

Figure 7. Linear attenuation coefficient of the fabricated glass.

Table 5. Experimental values of LAC, MAC, HVL, TVL and MFP of ((100-y){85[25(glass sand)+35H_3BO_3+ 40Na_2CO_3]+15BaO}y[$Bi_2(CO_3)O_2$]) glasses.

Samples (Y)	Gamma source point for Caesium (Cs-137) 661.7KeV				
	LAC (cm^{-1})	MAC (cm^2/g)	HVL (cm)	TVL (cm)	MFP (cm)
5	0.198255	0.067895	3.496246	11.61428	5.044017
10	0.198255	0.065387	3.496246	11.61428	5.044017
15	0.115706	0.036363	5.990587	19.9003	8.64259
20	0.246322	0.072704	2.813989	9.347868	4.059728
25	0.268437	0.076002	2.582157	8.577739	3.725265

Table 6. Experimental values of LAC, MAC, HVL, TVL and MFP of ((100-y){85[25(glass sand)+35H_3BO_3+ 40Na_2CO_3]+15BaO}y[$Bi_2(CO_3)O_2$]) glasses.

Samples (Y)	Gamma source point for Cobalt-60 (1253KeV)				
	LAC (cm^{-1})	MA (cm^2/g)	HVL (cm)	TVL (cm)	MFP (cm)
5	0.282923	0.096891	2.449954	8.138571	3.534536
10	0.277113	0.091396	2.501314	8.309184	3.608633
15	0.129695	0.040759	5.344431	17.75381	7.710383
20	0.239971	0.07083	2.888461	9.59526	4.167168
25	0.338657	0.095882	2.046755	6.799175	2.952844

two gamma sources which are 0.115706 and 0.129695 cm^{-1}. However, bismuth ore (bismutite) $Bi_2O_2CO_3$ enhances the gamma absorption ability of the study glasses.

The introduction of a $Bi_2O_2CO_3$ into the glass matrix due to its high atomic weight and density influences the increase in LAC (Kundu *et al*., 2014). This is because the chance of photon interactions in denser materials is reasonably higher than with less dense material (Muwazanat

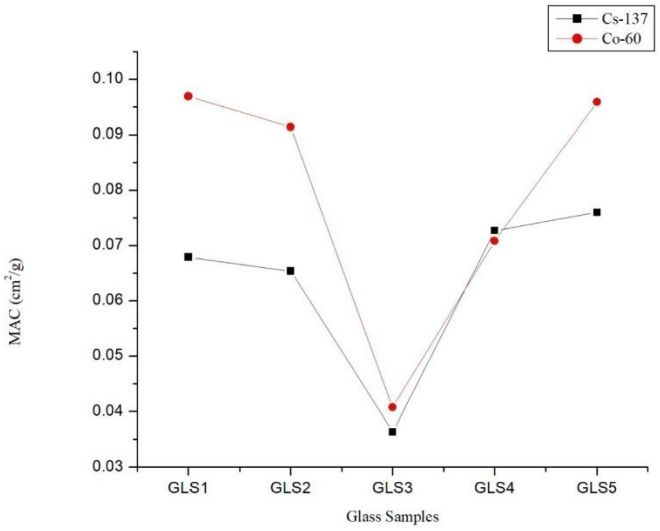

Figure 8. Mass attenuation coefficient of the fabricated glass.

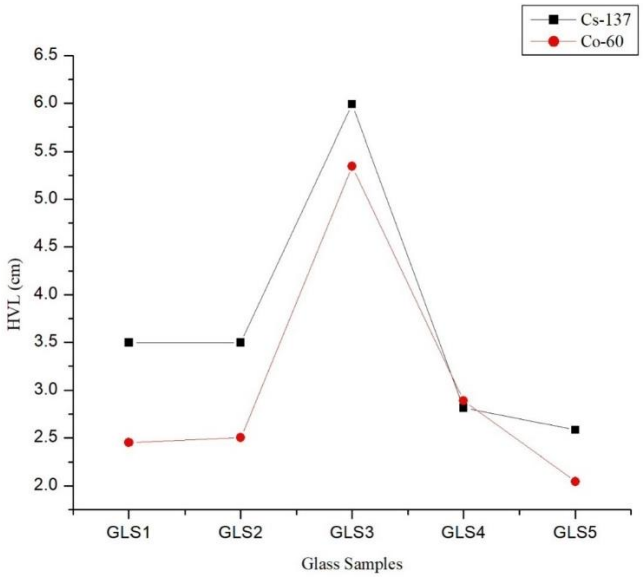

Figure 9. Half value layer of the fabricated glass.

and Pertimbangan, 2022).

Figure 8, Tables 5 and 6 shows the respective values of MAC are given as 0.067895, 0.065387, 0.036363, 0.072704 and 0.076002 cm^2/g for GLS5, GLS10, GLS15, GLS20 and GLS25 (Caesium-137) and 0.096891, 0.091396, 0.040759, 0.07083 and 0.095882 cm^2/g for GLS5, GLS10, GLS15, GLS20 and GLS25 (Cobalt-60) respectively. As the content of bismutite ($Bi_2O_2CO_3$) changes from 5 to 25 wt. %, the values of MAC at energy (661KeV) and energy (1235KeV) show a similar decreasing and increasing behaviour as exhibited by LAC. The observed increase in MAC of the prepared glasses might be linked with an increase in glass effective density

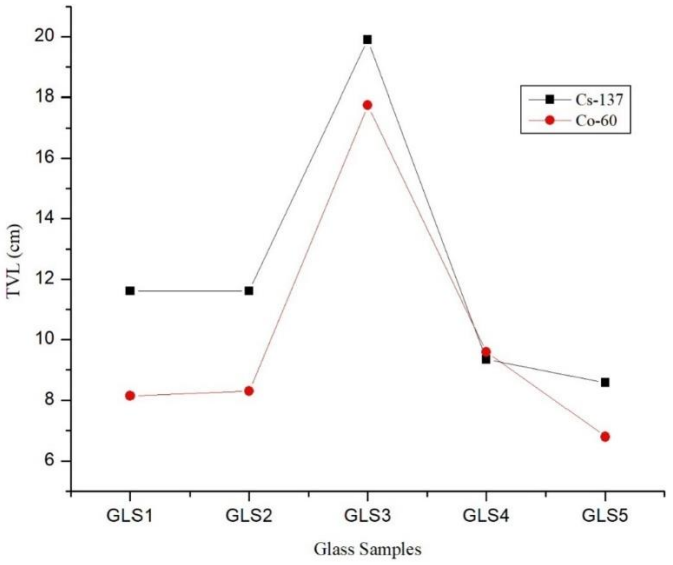

Figure 10. Tenth value layer of the fabricated glass.

as well as mass density, which thereby results in a high probability of photon interaction (Han *et al*., 2021; Olarinoye *et al*., 2020).

Half Value Layer (HVL) Tenth Value Layer (TVL) Mean Free Path (MFP) of (100-y){85[25(glass sand)+35H_3BO_3 +40Na_2CO_3]+15BaO}y[$Bi_2(CO_3)O_2$] glasses

The Half Value Layer and Tenth Value Layer refer to the thickness of the absorber needed to reduce the intensity of gamma radiation to half and tenth of its initial intensity (Lacomme *et al.,* 2021). These are very important factors to consider when assessing a material's ability to shield.

Figures 9 and 10 demonstrate the variation of HVL and TVL of (100-y){85[25(glass sand)+35H_3BO_3+40Na_2CO_3]+ 15BaO}y[$Bi_2(CO_3)O_2$] of the glass system as a function bismutite ($Bi_2O_2CO_3$) weight percentage (wt. %). It appears that when the weight percentage of bismutite ($Bi_2O_2CO_3$) increases from 5 to 25 weight per cent, the values of HVL and TVL for Caesium-137 increase from 2.449954 cm to 5.344431 then decrease to 2.046755 cm (HVL) and 8.138571 cm to 17.75381cm to 6.799175 cm (TVL), respectively, as shown in Tables 5 and 6. These results show that the samples doped with a greater weight per cent of $Bi_2O_2CO_3$ have the lowest HVL and TVL values for Caesium-137 (2.582157 cm and 8.577739 cm) and Cobalt-60 (2.046755 cm and 6.799175 cm). A drop in HVL and TVL for the two gamma sources is a direct result of a density increase (Rammah *et al*., 2021). HVL and TVL values are lower in good shielding materials (Lacomme *et al*., 2021).

The Mean Free Path (MFP) is the average distance travelled between two consecutive photon interactions, expressed mathematically as an inverse of LAC. MFP=

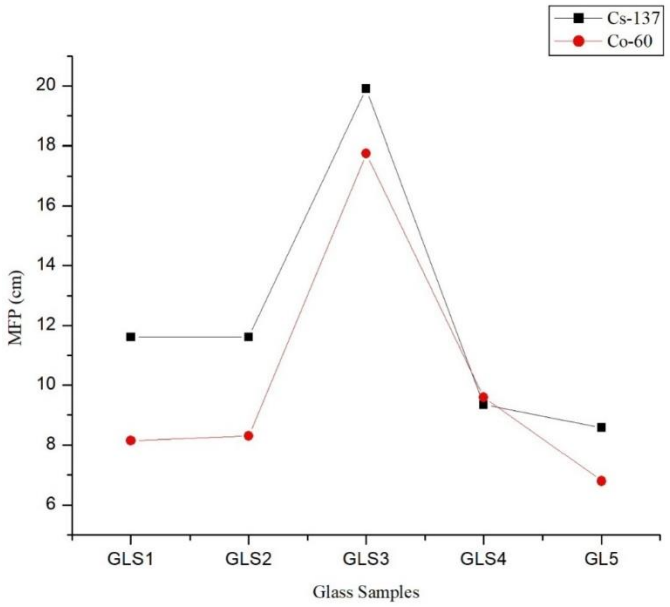

Figure 11. Experimental mean free path of the fabricated glass.

LAC^{-1} (Elsafi et al., 2021; Elmahroug *et al*., 2018).

Figure 11, Tables 5 and 6 illustrate the variation of MFP against $Bi_2O_2CO_3$ weight percentage of (100-y){85[25(glass sand)+35H_3BO_3+40Na_2CO_3]+15BaO}y[$Bi_2(CO_3)O_2$] glasses. The values of MFP for GLS5 (5.044017 cm), GLS10 (5.044017 cm), GLS15 (8.64259 cm), GLS20 (4.059728 cm) and GLS25 (3.725265 cm) for Caesium-137. MFP values for Cobalt-60 are 3.534536cm (GLS5), 3.608633 cm (GLS10), 7.710383 cm (GLS15), 4.167168 cm (GLS20), and 2.952844 cm (GLS25). The MFP for both Cobalt-60 and Caesium-137 is comparable to HVL and TVL. With the exception of GLS15, which has the highest MFP (8.64259 cm) for Caesium-137 and the lowest MFP (2.952844cm) for Cobalt-60, the MFP values decrease as the amount of bismuth ore ($Bi_2O_2CO_3$) increases, totalling between 5 and 25 weight per cent. It also has the greatest LAC and density values among the created glass samples.

Conclusion

Using the melt quench process, Glass Sand ore doped with Bismutite and barium oxide with a chemical composition of (100-y) 85[25(glass sand)-35B_2O_3-40Na_2CO_3)15BaO]($Bi_2O_2CO_3$)y, y = 5, 10, 15, 20, 25 weight percentage, was fabricated. The glass sand's silica content was confirmed to be 78.99% by the X-ray fluorescence (DEXRF) result. It has been determined that the density of the glass samples increased proportionately from 2.919 to 3.532 g/cm^3 when the concentration of bismuth ore (bismutite) increased. The glasses were confirmed amorphous as the XRD pattern revealed, while the FTIR analysis showed the presence of BO_3 and SiO_4 structural units. The Gamma-Ray attenuation experiment of radiation shielding parameters was carried out on all glass samples effectiveness using two radioactive gamma point sources, namely, Caesium-137 and Co-60. The glasses have higher gamma attenuation effectiveness than Pb/Ba glass that is sold commercially. It was discovered that the glass attenuated photons with a mean energy of 1253 keV by 661.7 keV. Depending on the glass density, the refractive indices of the glass series rise as the concentration of the $Bi_2O_2CO_3$ fraction in the glass system increases. The refractive index rises as the glass gets denser because less light travels through the sample at that speed. The LAC decreases and increases at different weight percentages ranging from 5 to 25%, GLS25 for the two sources have the highest LAC (0.268437 cm^{-1} and 0.338657 cm^{-1}) while the least LAC was observed at GLS15 for the two gamma sources which are 0.115706 and 0.129695 cm^{-1}. As the content of bismutite ($Bi_2O_2CO_3$) changes from 5 to 25 wt. %, the values of MAC at energy (661KeV) and energy (1235KeV) show a similar decreasing and increasing behaviour as exhibited by LAC. The values of HVL and TVL for Caesium-137 increase from 2.449954 to 5.344431 then decrease to 2.046755 cm (HVL) and 8.138571 to 17.75381 to 6.799175 cm (TVL), respectively. These results show that the samples doped with a greater weight per cent of $Bi_2O_2CO_3$ have the lowest HVL and TVL values for Caesium-137 (2.582157 and 8.577739 cm) and Cobalt-60 (2.046755 and 6.799175 cm). A drop in HVL and TVL for the two gamma sources is a direct result of a density increase. HVL and TVL values are lower in good shielding materials. The MFP for both Cobalt-60 and Caesium-137 is comparable to HVL and TVL, with the exception of GLS15, which has the highest MFP (8.64259 cm) for Caesium-137 and the lowest MFP (2.952844 cm) for Cobalt-60.

CONFLICT OF INTEREST

The authors declare that they have no conflict of interest.

REFERENCES

Abdul Aziz, S. H., El-Mallawany, R., Badaron, S. S., Kamari, H. M., & Amin Matori, K. (2015). Optical properties of erbium zinc tellurite glass system. *Advances in Materials Science and Engineering*, *2015*(1), 628954.

Acevedo-Del-Castillo, A., Águila-Toledo, E., Maldonado-Magnere, S., & Aguilar-Bolados, H. (2021). A brief review on the high-energy electromagnetic radiation-shielding materials based on polymer nanocomposites. *International Journal of Molecular Sciences*, *22*(16), 9079.

Alazoumi, S. H., Sidek, H. A. A., Halimah, M. K., Matori, K. A., Zaid, M. H. M., & Abdulbaset, A. A. (2017). Synthesis and elastic properties of ternary ZnO-PbO-TeO_2 glasses. *Chalcogenide Letters*, *14*(8), 303-320.

Al-Buriahi, M. S., Rashad, M., Alalawi, A., & Sayyed, M. I. (2020). Effect of Bi_2O_3 on mechanical features and radiation shielding properties of boro-tellurite glass system. *Ceramics International*, *46*(10), 16452-16458.

Aliyu, U. S., Kamari, H. M., Hamza, A. M., & Awshah, A. A. (2018). The structural, physical and optical properties of borotellurite glasses incorporated with silica from rice husk. *Journal of Science and Mathematics Letters*, *6*, 32-46.

Andreeva, P., Stoilov, V., & Petrov, O. (2011). Application of X-Ray diffraction analysis for sedimentological investigation of Middle Devonian dolomites from Northeastern Bulgaria. *Geologica Balcanica*, *40*(1-3), 31-38.

Bale, S., Rahman, S., Awasthi, A. M., & Sathe, V. (2008). Role of Bi_2O_3 content on physical, optical and vibrational studies in Bi_2O_3-ZnO-B_2O_3 glasses. *Journal of Alloys and Compounds*, *460*(1–2), 699-703.

Baptista Neto, A. T., & Faria, L. O. (2014). Construction and calibration of a multipurpose instrument to simultaneously measure dose, voltage and half-value layer in X-ray emission equipment. *Radiation Measurements*, *71*, 178-182.

Berwal, N., Dhankhar, S., Sharma, P., Kundu, R. S., Punia, R., & Kishore, N. (2017a). Physical, structural and optical characterization of silicate modified bismuth-borate-tellurite glasses. *Journal of Molecular Structure*, *1127*, 636-644.

Bunaciu, A. A., Udriştioiu, E. gabriela, & Aboul-Enein, H. Y. (2015). X-ray diffraction: instrumentation and applications. *Critical Reviews in Analytical Chemistry*, *45*(4), 289-299.

Causin, V., Marega, C., Marigo, A., Casamassima, R., Peluso, G., &Ripani, L. (2010). Forensic differentiation of paper by x-ray diffraction and infrared spectroscopy. *Forensic Science International*, *197*(1–3), 70-74.

Chanthima, N., Kaewkhao, J., Kedkaew, C., Chewpraditkul, W., Pokaipisit, A., &Limsuwan, P. (2011). Study on interaction of Bi_2O_3, PbO and BaO in silicate glass system at 662 keV for development of gamma-rays shielding materials. *Progress in Nuclear Science and Technology*, *1*(0), 106-109.

Deepty, M., Srinivas, C., Kumar, E. R., Mohan, N. K., Prajapat, C. L., Rao, T. V. C.,Meena, S. S., Verma, A. K., & Sastry, D. L. (2019). XRD, EDX, FTIR and ESRS pectroscopic studies of Co-precipitated Mn–substituted Zn–ferrite nanoparticles. *Ceramics International*, *45*(6), 8037-8044.

Connolly, J. R. (2005). Introduction to X-ray powder diffraction. Spring. Pp. 1-9. Retrieved from http://www.xray.cz/xray/csca/kol2011/kurs/dalsi-cteni/connolly-2005/01-xrd-intro.pdf

Doweidar, H., El-Damrawi, G. M., Moustafa, Y. M., & Ramadan, R. M. (2005). Density of mixed alkali borate glasses: A structural analysis. *Physica B: Condensed Matter*, *362*(1-4), 123-132.

Dutrow, B. L. (2020). X-ray Powder Diffraction (XRD). In *Integrating Research and Education*. Pp.21-24. Retrieved from https://serc.carleton.edu/research_education/geochemsheets/techniques/XRD.html

Elmahroug, Y., Almatari, M., Sayyed, M. I., Dong, M. G., & Tekin, H. O. (2018). Investigation of radiation shielding properties for Bi_2O_3-V_2O_5-TeO_2 glass system using MCNP5 code. *Journal of Non-Crystalline Solids*, *499*, 32-40.

Elsafi, M., EL-Nahal, M.A., Sayyed, M.I., Saleh,I.H., & Abbas, M.I. (2021). Effect of bulk and nanoparticles Bi_2O_3 on attenuation capability of radiation shielding glass. *Ceramics International*, *47*(14), 19651-19658.

Gaikwad, D. K., Obaid, S. S., Sayyed, M. I., Bhosale, R. R., Awasarmol, V. V., Kumar, A., Shirsat, M. D., & Pawar, P. P. (2018). Comparative study of gamma ray shielding competence of WO_3-TeO_2-PbO glass system to different glasses and concretes. *Materials Chemistry and Physics*, *213*, 508-517.

Halimah, M. K., Umar, S. A., Chan, K. T., Latif, A. A., Azlan, M. N., Abubakar, A. I., & Hamza, A. M. (2019). Study of Rice Husk Silicate Effects on the Elastic, Physical and Structural Properties of Borotellurite Glasses. *Materials Chemistry and Physics*, *238*, 121891.

Han, T., Sun, X. Y., Lai, X., Yu, J., Xia, L., Guo, H., & Ye, X. (2021). Role of Gd_2O_3 on tailoring structural and optical properties of Tb^{3+}-activated borogermanate-tellurite glasses. *Radiation Physics and Chemistry*, *189*, 109734.

IAEA (2019). Postgraduate Education Course in Radiation Protection and Safety of Radiation Sources: Standard Syllabus. *Training Course Series*, *18*, 12-14.

Jawad, A. A., Demirkol, N., Gunoğlu, K., & Akkurt, I. (2019). Radiation shielding properties of some ceramic wasted samples. *International Journal of Environmental Science and Technology*, *16*, 5039-5042.

Kolanoski, H., & Wermes, N. (2020). Introduction. In *Particle Detectors: Fundamentals and Applications*. Oxford University Press. Pp. 1-2. Retrieved from https://doi.org/10.1093/oso/9780198858362.003.0001.

Kumar, A., Gaikwad, D. K., Obaid, S. S., Tekin, H. O., & Sayyed, M. I. (2020). Experimental studies and monte carlo simulation on gamma ray shielding competence of (30+X) Pb-10WO_3-10Na_2O-10MgO-(40-X)B_2O_3 Glasses. *Progress in Nuclear Energy*, *119*, 103047.

Kundu, R. S., Dhankhar, S., Punia, R., Nanda, K., & Kishore, N. (2014). Bismuth modified physical, structural and optical properties of mid-IR transparent zinc boro-tellurite glasses. *Journal of Alloys and Compounds*, *587*, 66-73.

Lacomme, E., Sayyed, M. I., Sidek, H. A. A., Matori, K. A., & Zaid, M. H. M. (2021). Effect of bismuth and lithium substitution on radiation shielding properties of zinc borate glass system using Phy-X/PSD simulation. *Results in Physics*, *20*, 103768.

Mariyappan, M., Marimuthu, K., Sayyed, M. I., Dong, M. G., & Kara, U. (2018). Effect Bi_2O_3 on the physical, structural and radiation shielding properties of Er^{3+} ions doped bismuth sodium fluoroborate glasses. *Journal of Non-Crystalline Solids*, *499*, 75-85.

McCaffrey, J. P., Shen, H., Downton, B., &Mainegra-Hing, E. (2007). Radiation attenuation by lead and nonlead materials used in radiation shielding garments. *Medical Physics*, *34*(2), 530-537.

Naseer, K. A., Marimuthu, K., Mahmoud, K. A., & Sayyed, M. I. (2021). Impact of Bi_2O_3 modifier concentration on barium-zincborate glasses: physical, structural, elastic, and radiation-shielding properties. *European Physical Journal Plus*, *136*, 116.

NDT (2017). Resource Education Center. https;//www.cnde.iastate.edu'ndt

Obaid, S. S., Gaikwad, D. K., &Pawar, P. P. (2018). Determination of gamma ray shielding parameters of rocks and concrete. *Radiation Physics and Chemistry*, *144*, 356n-360.

Olarinoye, I. O., El-Agawany, F. I., EL-Adaw, A., Yousef, E. S., & Rammah, Y. S. (2020). Mechanical features, alpha particles, photon, proton and neutron interaction parameters of TeO_2-V_2O_3-MoO_3 semiconductor glasses. *Ceramics International*, *46*(14), 3134-23144.

Rachniyom, W., Ruangtaweep, Y., Kaewkhao, J., Ruengsri, S., &Phachana, K. (2014). Effects of Na_2O on borosilicate glasses prepared from coal fired ash. *Advanced Materials Research*, *979*, 271-274.

Rammah, Y. S., El-Agawany, F. I., Gamal, A., Olarinoye, I. O., Ahmed, E. M., Abuohaswa, A. S. (2021). Responsibility of Bi_2O_3 content in photon, alpha, proton, fast and thermal neutron shielding capacity and elastic moduli of zinc/B_2O_3/Bi_2O_3 glasses. *Journal of Inorganic and Organometallic*

Polymers and Materials, *31*(8), 3505-3524.

Sarachai, S., Chanthima, N., Sangwaranatee, N. W., Kothan, S., Kaewjaeng, S., Tungjai, M., Djamal, M., & Kaewkhao, J. (2018). Radiation shielding properties of BaO-ZnO-B_2O_3 glass for x-ray room. *Key Engineering Materials*, *766*, 88-93.

Sarachai, S., Chanthima, N., Sangwaranatee, N. W., Kothan, S., Kaewjaeng, S., Tungjai, M., Djamal, M., & Kaewkhao, J. (2018). Radiation shielding properties of BaO-ZnO-B_2O_3 glass for x-ray room. *Key Engineering Materials*, *766*, 88-93.

Sayyed, M. I., Kaky, K. M., Gaikwad, D. K., Agar, O., Gawai, U. P., & Baki, S. O. (2019). Physical, structural, optical and gamma radiation shielding properties of borate glasses containing heavy metals (Bi_2O_3/MoO_3). *Journal of Non-Crystalline Solids*, *507*, 30-37.

Sekimoto, M., &Katoh, Y. (2015). Coloring characteristic of lead glass for x-ray irradiation. *New Journal of Glass and Ceramics*, *5*(3), 25-30.

Singh, S., Kumar, A., Singh, D., Thind, K. S., &Mudahar, G. S. (2008). Barium-borate-flyash glasses: As radiation shielding materials. *Nuclear Instruments and Methods in Physics Research, Section B: Beam Interactions with Materials and Atoms*, *266*(1), 140-146.